International Journal of Recent Engineering Research and Development (IJRERD)
ISSN: 2455-8761
www.ijrerd.com || Volume 11 – Issue 02 || Mar - Apr 2026 || PP. 01-06

Numerical Study on the Effect of Fiber Grid Size on Shear Failure at Earthen Composite Interfaces

Mingwei Wang[1], Xuehuan Liang[2], Feng Wu[3]
[1,2.3]*School of Transportation Engineering, Dalian Jiaotong University, Dalian 116028, China*

Abstract: Failure of the fiber-reinforced earthen matrix (FREM) composite system is mostly controlled by interfacial shear debonding. Most current studies focus on improving the macroscopic bearing capacity of modified materials, while there is still a lack of research on the influence of geometric parameters of fiber grids on mesoscopic stress redistribution and the transformation mechanism of failure modes in low-modulus earthen matrix. Based on the double-interface nonlinear constitutive model, this paper establishes a three-dimensional refined finite element model of the FREM system. This paper systematically investigates and clarifies the control law of glass fiber grid spacing on the evolution of interfacial stress transfer regions and failure modes through the model. The model verification results show that the numerical framework established in this paper can accurately simulate the nonlinear load-slip response under shear loading. Parametric analysis results show that when the grid spacing increases from 10 mm to 20 mm, the interfacial failure mode changes from brittle "matrix-surface layer debonding" to "local fiber rupture". The reason for this transition is that the decrease in grid density leads to severe stress localization, which causes single fibers to rupture due to overload and prevents the effective transfer of shear stress to the deep matrix. This study quantifies the matching relationship between fiber tensile strength and matrix shear strength, and provides a theoretical reference for the mesoscopic optimization design of composite reinforcement systems for earthen buildings.

Keywords: Earthen； Composites； Glass fiber mesh； Interface bonding； Numerical modelling

1. Introduction

Fiber-reinforced earthen matrix (FREM) is an external reinforcement technology with excellent compatibility, shows significant potential in the restoration and seismic reinforcement of traditional earthen structures[1]. By coating a modified earthen layer on the surface of the earthen matrix and embedding high-strength fiber mesh in the modified earthen layer, this system can significantly improve the in-plane shear resistance and out-of-plane bending resistance of original earthen walls. However, compared with traditional high-strength fiber-reinforced cementitious matrix composites (FRCM), there is an obvious physical and mechanical mismatch in the FREM system: the stiffness difference between the low-modulus, low-strength earthen matrix and high-modulus glass fiber is large[2]. This causes the failure of the FREM system to usually occur before the tensile strength of fibers is fully exerted, in the form of debonding at the interface between the surface layer and the matrix or slippage of the fiber mesh[3].

In recent years, to break through the bottleneck of low performance of earthen materials, scholars have tried to add modified materials such as hydraulic lime and waterborne polyurethane to improve the mechanical properties of the surface layer and the matrix[4]-[5]. However, the interfacial shear transfer efficiency is not only affected by the constitutive properties of materials, but the geometric layout, mesh spacing and density of fiber mesh are also key physical quantities that affect the interfacial stress transfer path and fracture energy dissipation. In TRM/FRCM systems with cement mortar as the matrix, studies have confirmed that the aperture size of fiber mesh directly determines the "mechanical interlocking" ability of the matrix mortar between meshes[6]. However, due to its special characteristics such as high plasticity and low strength, the earthen matrix has essentially different meso-mechanical effects at internal interfaces from cement-based materials, so conventional interfacial shear lag models are difficult to apply directly.

At present, macroscopic single or double shear tests can obtain macroscopic load-slip curves, but it is difficult to observe the stress redistribution process and damage evolution path inside fibers and deep at the interface in situ. Therefore, this study constructs a three-dimensional refined nonlinear finite element model and conducts in-depth microscopic theoretical analysis for geometric variables with fiber mesh spacing of 10 mm and 20 mm. This paper studies the diffusion mechanism of interfacial shear stress and the migration characteristics of stress transfer regions under different fiber mesh spacings, so as to reveal the internal mechanical mechanism of the failure mode transition at FREM interfaces caused by the geometric effect of fiber mesh.

2. Numerical modeling

2.1 Model building

To accurately capture the meso-mechanical response of the interface, this paper uses a discrete modeling method to rebuild the single shear bonding test process. The model has three parts: matrix, modified earthen surface layer and glass fiber mesh. Taking the ANN-200 specimen as an example, the matrix size is 260 mm × 100 mm × 100 mm; the surface layer size is 200 mm × 60 mm × 10 mm; the fiber mesh is a solid element of 350 mm × 60 mm × 0.2 mm. To reduce stress concentration and improve calculation convergence, a rigid part of 80 mm × 60 mm × 10 mmis placed on the top of the fiber mesh at the loading end. The schematic diagram of the specimen is shown in Figure 1.

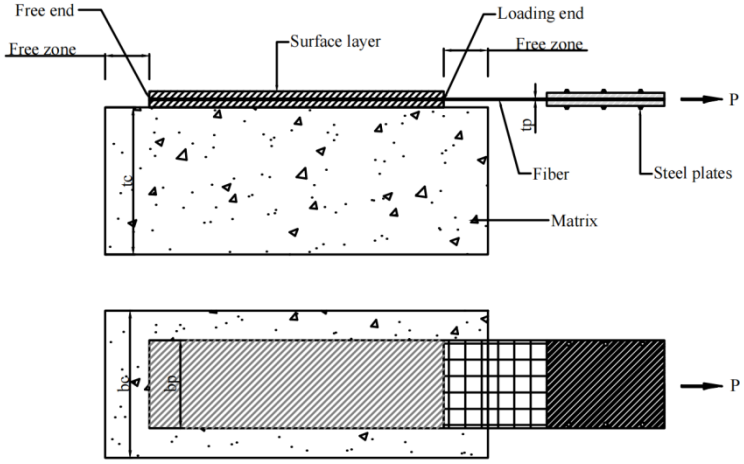

Figure 1: Structural schematic diagram of the specimen

Researchers have found that the constitutive relationship of earthen materials is similar to that of concrete[7]. The material parameters in this study were derived from preliminary experiments conducted by our research team. The elastic moduli of artificial hydraulic lime-modified earthen material and natural hydraulic lime-modified earthen material were 102.36 MPa and 79.87 MPa, respectively, with Poisson's ratios both being 0.3. Their ultimate tensile strengths were 0.192 MPa and 0.145 MPa, respectively, and the peak load strains were 0.0141 and 0.0103, respectively. The glass fiber mesh is produced by Taishan glass fiber company, with a standard mesh spacing of 10mm. The average elastic modulus of six glass fiber bundles is 8104.29 MPa. Their ultimate tensile strength is 303.73 MPa, and their ultimate tensile force is 1393.13 N. In this paper, the matrix, modified earthen surface layer and glass fiber mesh all use 8-node linear brick elements (C3D8R). To balance calculation efficiency and accuracy[8], the global mesh size of the matrix and surface layer is set to 5 mm. The fiber mesh area sensitive to stress gradient is locally refined, with a mesh size of 1 mm.

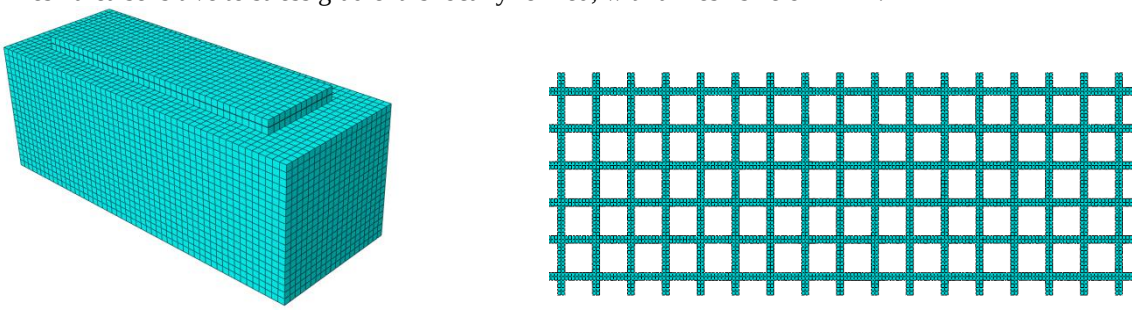

(a) (b)

Figure2: Grid size: (a) Matrix and surface layer; (b) Glass fiber mesh

2.2 Interface constitutive relationship

The accuracy of the model largely depends on the definition of interface behavior. Therefore, the parameters of the "matrix-surface layer" interface in this paper are calibrated and extracted directly from direct shear test data. For the "surface layer-fiber mesh" interface, a tri-linear bond-slip constitutive model is adopted. This model covers the whole process from elastic bonding, damage softening to full frictional slip. The mathematical expression of the interfacial bond-slip constitutive model is as follows:

$$f(s)=\begin{cases}\dfrac{\tau_f}{s_1}s & 0\le s\le s_1\\ \dfrac{\tau_f}{s_2-s_1}(s_2-s)s_1<s\le(1-A)s_2+As_1\\ A\tau_f(1-A)s_2+As_1<\mathrm{s}\le s_f\\ 0 & s>s_f\end{cases}$$

Where: τ_f is the peak stress (MPa); S_1 is the corresponding slip at the peak point (mm); A τ_f represents the debonding initiation stress of the fiber (MPa); s_f is the ultimate slip at complete interfacial failure (mm), beyond which the interfacial bond stress is completely lost.

For ANN-200 and ANA-200, the maximum shear stress τ_f in the elastic stage is 0.34 MPa and 0.84 MPa, respectively, with corresponding relative slip S_1 of 0.63 mm and 0.56 mm. The constant shear stress after complete debonding is 0.0014 MPa and 0.017 MPa, respectively, and the total slip is 1.38 mm and 1.36 mm.

2.3 Model validation

This paper takes the hydraulic lime modified system as an example. It conducts numerical simulations on ANN-200 and ANA-200 specimens. The load-slip curves obtained by finite element analysis agree well with the test results in the elastic ascending stage, the peak point and the brittle descending stage after debonding. In addition, the stress map reproduces the migration process of shear stress from the loading end to the free end.

As shown in Figure 3, the load-slip curve obtained from the ANA-200 specimen simulation agrees well with the test curve in the ascending stage, near the peak load and the descending stage. The curve drops sharply after reaching the peak, which shows the characteristic of brittle debonding. It also presents the transfer and redistribution of interfacial shear stress in the matrix from the loading end to the free end during loading. At the initial loading stage, shear stress mainly concentrates near the loading end. With the increase of load, the stress gradually moves toward the free end, but still gathers near the loading end. The stress at the free end is close to 0, which means the stress transfer length is much shorter than the anchorage length.

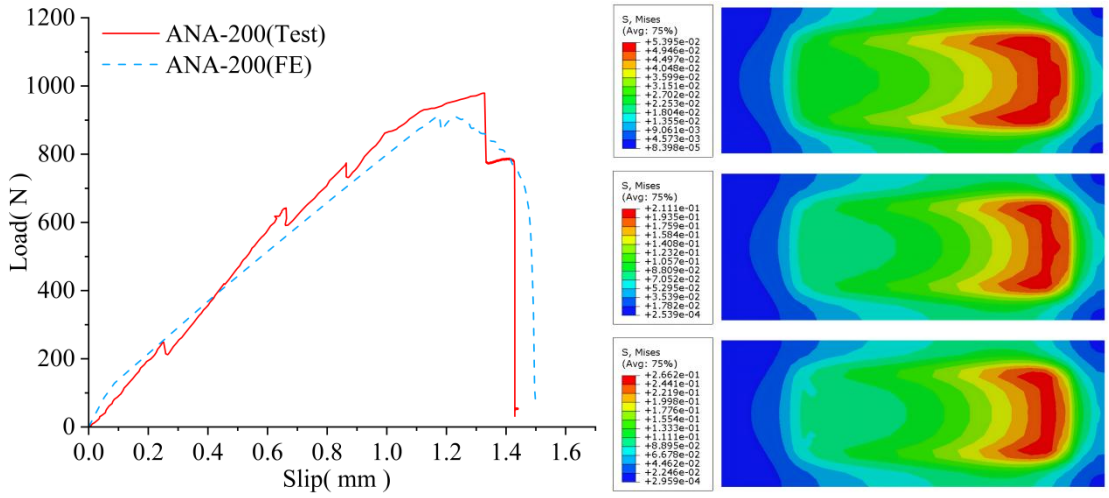

Figure 3: ANA-200 load-slip curve and stress distribution diagram.

Figure 4 shows the comparison results of the ANN-200 specimen. The simulated load-slip curve of this specimen fits well with the test curve in the elastic ascending stage. The overall shape of the curve and the descending stage after the peak are basically consistent with the test, and both show typical brittle failure characteristics. The stress distribution map shows that the interfacial shear stress is also concentrated in the loading end area. However, the stress peak is lower than that of ANA-200, which is consistent with the lower mechanical properties of the natural hydraulic lime modified surface layer.

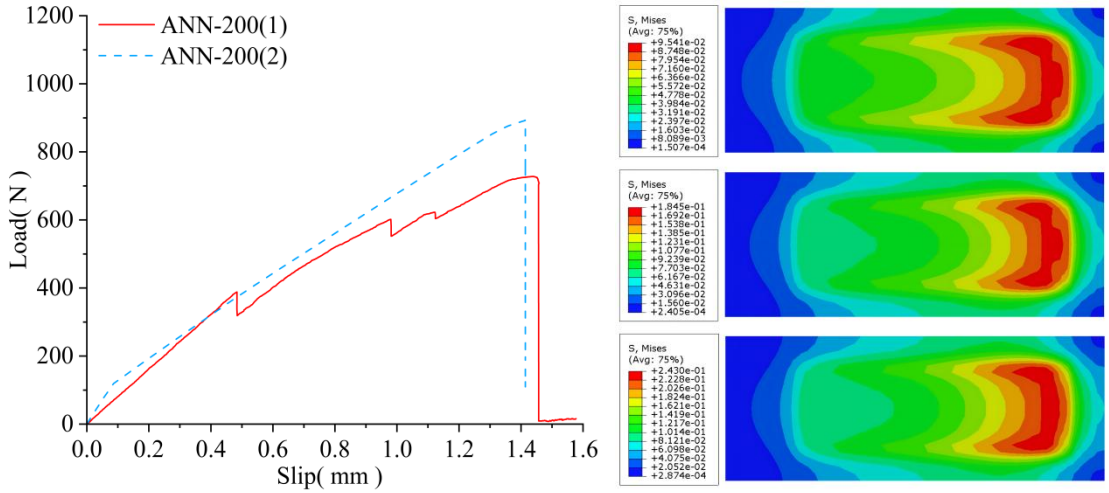

Figure 4: ANN-200 load-slip curve and stress distribution diagram.

3. Discussion on mesh size effect and meso-scale failure mechanism

Based on the accurate prediction of the numerical model, this paper excludes the interference caused by material modification. It strictly controls the single geometric variable and studies the meso control mechanism of 10 mm and 20 mm fiber mesh spacing on the failure mode of the FREM system. According to the recommendation of RILEM[8], the surface layer should contain at least three fiber bundles when its total width remains unchanged. Based on the verified finite element model, parametric numerical simulation is carried out for specimens with 20 mm fiber mesh spacing. The load-slip curves of ANN-200 and ANA-200 specimens with 20 mm fiber mesh spacing are shown in Figure 5.

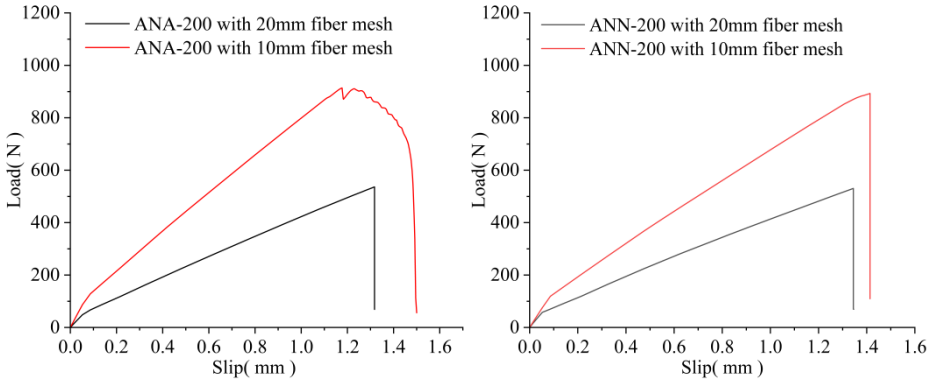

Figure 5: Load-slip curves of specimens with different fiber mesh spacing: (a) ANA-200; (b) ANN-200

3.1 Transition of failure mode

Numerical simulation results show a key phenomenon. Increasing fiber mesh spacing changes the interface failure mode and load transfer mechanism. Taking the ANA-200 specimen as an example, the failure mode is matrix-surface layer debonding at 10 mm mesh spacing. When the mesh spacing increases to 20 mm, the failure mode changes to fiber rupture. Similarly, the failure mode of the ANN-200 specimen also changes from matrix-surface layer debonding at 10 mm to fiber rupture at 20 mm. This phenomenon is mainly because larger mesh spacing reduces the number of fibers within the same surface layer width, so the load on each single fiber increases accordingly.

In the dense case with 10 mm fiber mesh spacing, the whole loading process shows an obvious "strong fiber-weak interface" characteristic. According to the fiber axial stress extracted from the model, when the ANA-200 specimen reaches the ultimate load, the axial tensile stress of its internal glass fiber mesh is far below the tensile strength limit of the material. At this time, interface damage mainly occurs between the earthen matrix and the surface layer, leading to typical large-area brittle debonding between the matrix and the surface layer in the specimen.

However, when the total width of the surface layer is kept at 60mm and the fiber mesh spacing is increased to 20 mm, the number of longitudinal main fiber bundles is reduced by half. Specimens with the same

material configuration do not show the expected overall interface slip. Instead, at a small macroscopic slip, the fiber stress at the root of the loading end quickly reaches the yield state and causes local fiber rupture. The transition from interface debonding to fiber rupture means a fundamental change in the load transfer mechanism of the system.

3.2 Interface stress redistribution and evolution mechanism

The transition in failure mode is not accidental. Its underlying mechanical cause lies in the stress localization and the change of stress transfer region caused by the reduction of mesh density. In the surface layer with a fixed width of 60mm, increasing the mesh spacing from 10 mm to 20 mm significantly reduces the number of main fiber bundles directly resisting longitudinal shear. Under similar external tensile shear demands, each glass fiber has to bear a doubled axial tensile load. As shown in Figure 6, the peak stress of single fibers in the 20 mm mesh group reaches the ultimate physical strength of the material, accompanied by obvious stress concentration. In contrast to the uniform stress distribution in the dense 10 mm mesh, some fibers in the 20 mm mesh specimen rupture prematurely.

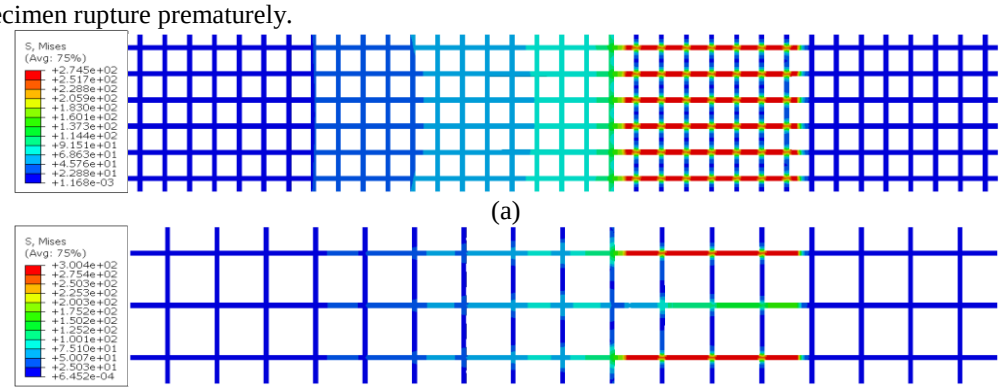

Figure 6: The peak stress of fiber of ANA-200 specimens: (a) at mesh spacing of 10 mm; (b) at mesh spacing of 20 mm

The dense 10mm mesh serves as a high-density stress-diffusion network on the earthen surface layer. Interfacial shear stress can spread uniformly in both transverse and longitudinal directions through these fine mesh openings, gradually forming a continuous, stable and wide stress transfer area. In this case, the earthen matrix penetrating the mesh openings is small in volume but evenly distributed, providing a stable mechanical interlocking effect for the system. Therefore, the weak point of the system is still dominated by the large-area earthen matrix with low shear strength.

In contrast, the sparse 20 mm mesh greatly weakens the lateral restraint effect of fibers. Shear stress cannot spread effectively to the surrounding area, resulting in high stress concentration at the loading-end root of the few main loaded fibers. Figure 7 shows the interfacial shear stress (ISS). It can be seen that the load-slip curve under the 20 mm mesh condition shows a local peak at the loading end, while that under the 10 mm mesh condition forms a continuous stress distribution. Meanwhile, obvious stress transfer toward the free end is observed under the 10 mm mesh condition, which is absent in the 20 mm mesh case.

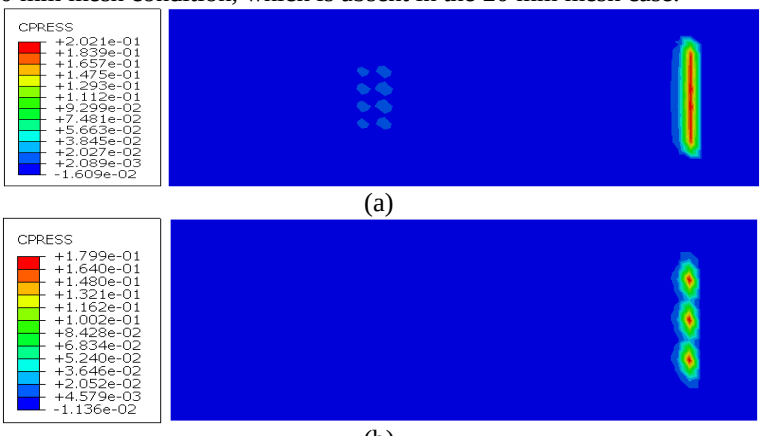

Figure 7: The interfacial shear stress of ANA-200 specimen: (a) at mesh spacing of 10 mm; (b) at mesh spacing of 20 mm

4. Conclusion

Based on 3D nonlinear finite element simulations, this paper for the first time analyzes the interfacial shear transfer mechanism of fiber-reinforced earthen matrix (FREM) composites from the perspective of meso-geometry. The main conclusions are as follows:

(1) Fiber mesh spacing is the key variable controlling the evolution of failure modes in FREM systems. Increasing the mesh spacing from 10 mm to 20 mm forces the system failure mechanism to change from macroscopic interfacial shear debonding to meso-scale local tensile rupture of single fiber bundles.

(2) A larger mesh spacing leads to a sharp increase in the load carried by single fibers, and the stress transfer paths of the fiber mesh become discrete, causing severe stress concentration at the loading end. This stress concentration weakens the synergistic interaction between fibers and the matrix, eventually resulting in a rapid drop in interfacial shear performance.

(3) In the design of FREM reinforcement systems, high-strength fibers should not be pursued blindly. A reasonable match between interfacial bond strength and fiber mesh density is the key to achieving synergistic load transfer and avoiding brittle fracture.

Reference

[1]. Gallipoli D, Bruno W A, Perlot C, et al. A geotechnical perspective of raw earth building [J]. Acta Geotechnica, 12 (3): 463-478, 2017.

[2]. Bui T, Bui Q, Limam A, et al. Failure of rammed earth walls: From observations to quantifications [J]. Construction and Building Materials, 51 295-302, 2014.

[3]. Weinan H, Feng W, Yuan C, et al. Compressive performance of adobe masonry strengthened with glass-fiber reinforced matrix composites [J]. Materials and Structures, 56 (3), 2023.

[4]. Wang Y, Niu F, Ding Z, et al. Experimental study of polyurethane cement composite–reinforced soft soil in the thawed layer in permafrost regions [J]. Construction and Building Materials, 420135622-, 2024.

[5]. Saleh S, Yunus M, Ahmad K, Ali N. Improving the strength of weak soil using polyurethane grouts: A review [J]. Constr Build Mater 202:738-752, 2019.

[6]. Xinxin D, Mingshuang Z, Hang L, et al. Bond Behaviors of Steel Fiber in Mortar Affected by Inclination Angle and Fiber Spacing [J]. Materials, 15 (17): 6024-6024, 2022.

[7]. F. Cai, Study on mechanical properties of the soil material with chemical reinforcement, Dalian Jiaotong University, Dalian, China, 2017.

[8]. X. Zhu, M. Su, Y. Wang, T. Ueda, Numerical and theoretical investigation on the constitutive model of graphene-enhanced FRCM composite, J. Build. Eng. 108734, 2024.

[9]. Felice D G, Aiello A M, Caggegi C, et al. Recommendation of RILEM Technical Committee 250-CSM: Test method for Textile Reinforced Mortar to substrate bond characterization [J]. Materials and Structures, 51 (4): 1-9, 2018.